Performance of a HL-LHC Nb_3Sn Quadrupole Magnet in the 100–200 MPa Range of Azimuthal Stress

F. J. Mangiarotti, S. Izquierdo Bermudez, A. Devred, *Senior Member, IEEE*, R. Diaz Vez, J. Ferradas Troitino, S. Ferradas Troitino, J. Feuvrier, M. Guinchard, A. Haziot, A. Milanese, S. Mugnier, J. C. Perez, P. Quassolo, S. Russenschuck, E. Todesco, and G. Willering

(Invited Paper)

***Abstract*—With the assembly and test results of four Nb_3Sn short-model quadrupoles (MQXFS) for the High Luminosity Upgrade of the CERN Large Hadron Collider (LHC), an optimum pre-load level was established for the construction of the full-length, series magnets. Successive MQXFS magnets were used as testbeds for potential changes (including pre-load fine tuning) to be implemented in the series, and to better understand the stress dependence of Nb_3Sn magnet performance. In this paper we report the findings of the short model MQXFS7, where we investigated the effect of higher azimuthal pre-load on the performance of this magnet assembled with coils wound from Nb_3Sn Restacked-Rod-Process (RRP) conductors, which are the baseline for MQXF magnets, and Powder-In-Tube (PIT) conductors, which were initially considered as a potential candidate but subsequently set aside. Starting at the baseline level of 110 MPa azimuthal preload at 1.9 K (corresponding to a full preload at nominal current, which is 77% of the short sample limit at 1.9 K), we increased the pre-load in steps of 20 MPa up to 190 MPa. The magnet was able to operate above 90% of the short sample limit indicating a large range of possible preloads. Indications of performance degradation at 90-95% of the short sample limit were found in the PIT conductor at 170 and 190 MPa. The test included a significant set of observables, such as the ramp rate dependency on the quench current, and V-I measurements to see growing resistance in segments of the coil.**

***Index Terms*—High stress, low beta quadrupole, Nb_3Sn, quench, superconducting magnets.**

I. Introduction

As PART of the High Luminosity LHC (HL-LHC) project at CERN, the inner triplet quadrupole magnets located near the ATLAS and CMS interaction points will be upgraded with larger aperture Nb_3Sn magnets, developed and manufactured in a collaboration between CERN and the US HL-LHC Accelerator Upgrade Project (AUP) [1]. These magnets, named MQXF, will generate a nominal gradient of 132.2 T/m in a 150 mm aperture at the nominal current of 16.23 kA, corresponding to a peak nominal magnetic field in the superconductors of 11.3 T. The cross section of the MQXF magnets is shown in Fig. 1, and a map of the magnetic field in the superconductors at nominal current is shown in Fig. 2.

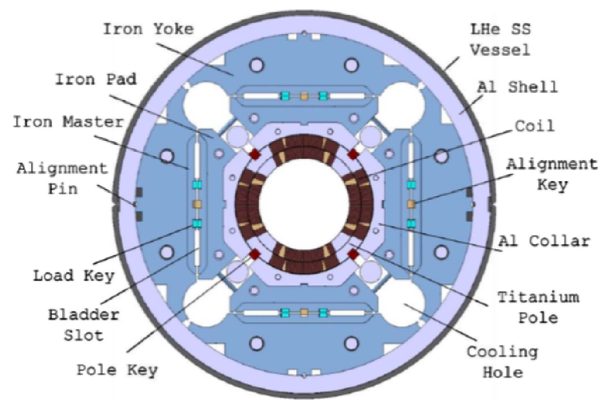

Fig. 1. Cross section of the MQXF magnet.

The mechanical assembly of these magnets is based on the *Bladder and Key* process [2]. The four superconducting coils are assembled inside a support structure relying on aluminum cylinders, and the desired mechanical pre-load to the coils is applied through a system of water-pressurized bladders and interference keys. Mechanical instrumentation is used to monitor the structural deformation (strain) of the magnet structure. The expected coil stress state is indirectly inferred from these experimental measurements based on numerical simulations [3]. Through this manuscript, we will quantify the azimuthal pre-load level at cryogenic temperature based on the pole unloading mechanism, as explained below.

To validate the design and manufacturing choices, several short-length model magnets (MQXFS) with the final cross-section design have been built and tested. The first four

Received 24 September 2024; accepted 15 November 2024. Date of publication 28 November 2024; date of current version 12 December 2024. *(Corresponding author: F. J. Mangiarotti.)*

F. J. Mangiarotti, S. Izquierdo Bermudez, A. Devred, R. Diaz Vez, J. Ferradas Troitino, J. Feuvrier, M. Guinchard, A. Haziot, A. Milanese, S. Mugnier, J. C. Perez, P. Quassolo, S. Russenschuck, E. Todesco, and G. Willering are with CERN, CH-1211 Geneva, Switzerland (e-mail: franco.julio.mangiarotti@cern.ch).

S. Ferradas Troitino was with CERN, CH-1211 Geneva, Switzerland. He is now with Advantics, Saint-Genis-Pouilly, 01630, France.

Color versions of one or more figures in this article are available at https://doi.org/10.1109/TASC.2024.3507751.

Digital Object Identifier 10.1109/TASC.2024.3507751

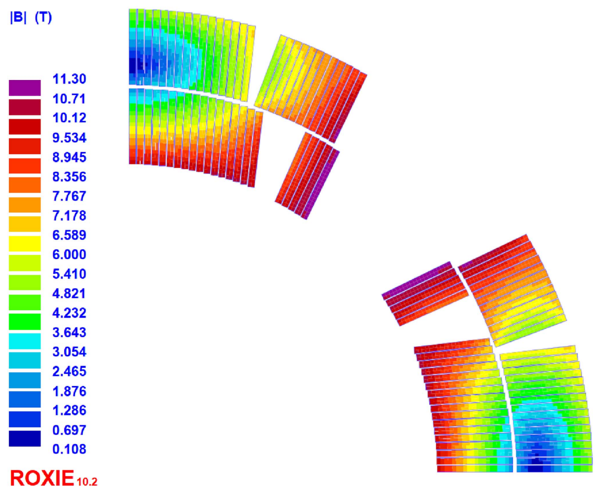

Fig. 2. Magnetic field in the superconductors in MQXF magnets, at nominal current. The peak field in the inner layer pole turn is 11.3 T.

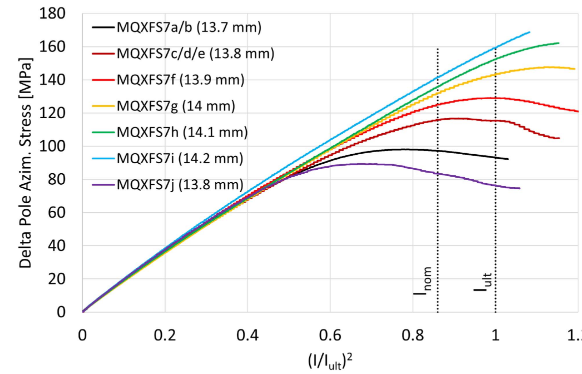

Fig. 3. Azimuthal pole stress as function of the square of the current normalized to the ultimate current in all MQXFS7 iterations. I_{nom} and I_{ult} correspond to nominal (16.23 kA) and ultimate current (17.5 kA) respectively. The numbers in brackets next to each magnet iteration corresponds to the loading key size.

short models magnets (MQXFS1 [4], [5], MQXFS3 [6], [7], MQXFS5 [6] and MQXFS4 [7], [8]), tested between 2015 and 2019, validated the main assembly parameters, including the pre-load level, which is currently used in the full-length series magnets [9].

Since the second half of 2019, the MQXFS magnets have been tested outside their design limits and nominal operation conditions: MQXFS4 was subject to a total of 10 cool-down and warm-up cycles to 1.9 K, more than 1000 current cycles to nominal current, and training 10% above nominal current. MQXFS6 was tested at the nominal azimuthal pre-load of 110 MPa, then at 65 MPa and one last time at 110 MPa, powered beyond nominal current up to a "quench plateau" (defined in the next section). The results of these tests are summarized in [8], [10]. In this manuscript we focus on MQXFS7, the latest MQXFS magnet.

A. History of MQXFS7

MQXFS7 is composed of four coils manufactured at CERN. Two of these coils (coils 113 and 114) were built with the final RRP conductor design that is used for the series production [11]. Another coil (coil 207) was built with PIT conductors without a bundle barrier, while the fourth coil (211) incorporated PIT conductors with bundle barrier [12].

The initial assembly, MQXFS7a, was built with a target azimuthal pre-load of approximately 100MPa at 1.9 K. The subsequent assembly, MQXFS7b, served to validate a new welding procedure for the stainless-steel vessel used in the MQXFB series magnets. This procedure was developed to minimize mechanical coupling between the outer stainless steel shell and the magnet structure [13]. Following testing, the stainless-steel vessel was removed, and the pole azimuthal pre-load was increased by replacing the 13.7 mm loading key with a 13.8 mm thick key, creating MQXFS7c. This additional 0.1 mm of interference raised the azimuthal pre-load to approximately 115 MPa.

As the new welding procedure required a fixed point between the stainless steel vessel and the magnet yoke, MQXFS7d was utilized to validate the new fixed point solution. In the next iteration, MQXFS7e, the new loading procedure implemented in MQXFB magnets was successfully demonstrated [9]. Subsequently, the loading key thickness was progressively increased in 0.1 mm increments across MQXFS7f, S7g, S7h, and S7i to examine the effects of varying pre-load levels, corresponding to azimuthal pre-loads at 1.9 K of 130, 150, 170, and 190 MPa, respectively.

In the final iteration, the loading key thickness was reduced to 13.8 mm, resulting in an azimuthal pre-load of 90 MPa, to determine whether the changes in magnet performance were reversible or irreversible. Fig. 3 shows the evolution of the variation in azimuthal pole stress (computed from strain measurements) during powering as a function of the square of the current. Beyond a certain point, a loss of linearity is observed, which is considered indicative of coil unloading from the pole and is used to experimentally assess the level of coil pre-load [3]. It is important to note that from MQXFS7e onwards, the only mechanical intervention performed on MQXFS7 was the increase of azimuthal pre-load. Therefore, MQXFS7e is used as the reference point for the stress studies presented in this paper.

II. Test Plan and Features

All iterations of MQXFS7 were tested at the superconducting magnet test facility SM18 at CERN. The magnet was mounted inside a vertical cryostat in SM18, where it was cooled down to 1.9 or 4.5 K in liquid helium at 1.3 bar. More information about the test benches used for MQXFS can be found in [6].

A. Magnet Instrumentation

All coils are instrumented with 8 voltage taps in each of their two layers, for a total of 64 voltage taps in each magnet. A schematic drawing of the voltage tap locations is shown in Fig. 4. The magnets are also instrumented with strain gauges on the shell, coils and rods, to monitor the strain and stress in the magnet during manufacturing and operation. See more information about these sensors in [14], [15], [16].

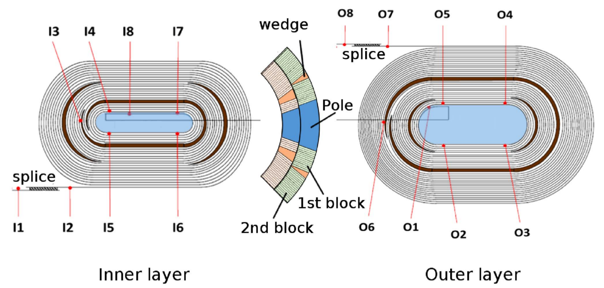

Fig. 4. Schematic drawing of the voltage taps location in MQXFS magnets. Voltage taps I5-I6 and I7-I8 cover the straight section of the inner layer pole turn. Voltage taps I8-O1 cover a part of the inner layer pole turn and the layer jump.

B. Magnet Protection

The magnet quench detection scheme was described in [6]. The baseline protection scheme for the full-size MQXF magnets includes outer layer quench heaters (OL-QH) and coupling-loss induced quench system (CLIQ) [17]; in MQXFS7 this protection scheme was only used in the initial training of the first iteration (MQXFS7a). For virtually all tests after the first training of MQXFS7a, the magnet was protected with OL-QH and an external energy extraction device (dump resistor) which extracts around 40-50% of the magnet stored energy to reduce the cryogenic load.

C. Test Procedure

Each test campaign started by cooling the magnet to 1.9 K in a superfluid helium bath. The magnet was first trained to either nominal current (only MQXFS7a) or up to a "quench plateau", defined as three or more quenches within 50 A of each other. This initial training at 1.9 K was always done at the nominal test ramp rate of 20 A/s. Once the training was completed, other tests were done at 1.9 K and also at 4.5 K in a saturated helium bath, including:

- Ramp rate studies: ramping the current up to quench at ramp rates between 50 and 400 A/s,
- V-I measurements: stepwise current increments up to quench, to measure small resistive voltages in sections of the coils

These standard tests have been made in most iterations of MQXFS7. In addition, additional tests were done in some MQXFS7 iterations:

- Thermal cycle: the thermal cycle is defined as a warm up from liquid helium to room temperature and cooling back down to 1.9 K. Thermal cycling is done without interventions in the magnet structure.
- Current cycles: in MQXFS7h, S7i and S7j we performed a large number of current cycles (300, 300 and 100 respectively) between 8 kA and ultimate current at 100 A/s to simulate mechanical fatigue.

III. Magnet Performance

A. Training

The training history of MQXFS7 at nominal test ramp rate is presented in Fig. 5 with the absolute current, and Fig. 6 normalized to the short sample limit (I_{ss}) of coil 211, which is the lowest among the four coils. At 1.9 K, the initial training of MQXFS7a up to ultimate current (the first 8 quenches) was done using OL-QH and CLIQ as protection scheme. Afterwards, all quenches were done with OL-QH and energy extraction for protection. MQXFS7a reaches nominal current after 4 quenches and ultimate current (17.50 kA) after 8 quenches. The training memory is kept after thermal cycle, and it reaches a maximum of 18.4 kA at the end of the second cool down. In MQXFS7b, the training memory after MQXFS7a is kept at the same level.

In MQXFS7c, the magnet trains at 1.9 K to a higher current level (19.2 kA) after increase of the azimuthal pre-load. This is similar to the observation in MQXFS6b-c-d that a lower-than-nominal pre-load causes a lower "quench plateau" at 1.9 K, and that increasing the pre-load back to nominal level allows the magnet to operate at a higher current [8]. Successive iterations also reach a "quench plateau" at 1.9 K in one or two quenches, with the exception of MQXFS7h which needed 5 quenches to reach it's plateau level. Note that, after the first training in MQXFS7a was completed, there were no quenches below ultimate current at 1.9 K. The quench plateau level at 1.9 K evolved from iteration to iteration; the average "quench plateau" value for each MQXFS7 iteration and cool down is shown in Fig. 7.

At 4.5 K, MQXFS7 does not train, but reaches a "quench plateau" immediately. As can be seen in Fig. 6, in most cases the fraction of short sample limit reached at 4.5 K is higher than at 1.9 K, and this is more pronounced in the initial MQXFS7 iterations. As such, we interpret the "quench plateau" level at 4.5 K as a better indicator of the performance of the superconducting strands and cables in the coil. The magnet performance at 4.5 K, similarly to that at 1.9 K, is degraded with successive magnet iterations, as shown in Fig. 7. Note that the maximum fraction of short sample limit reached at 4.5 K is 98% in MQXFS7b, and at the end of the MQXFS7j tests it reached up to 90%.

Thermal cycles do not change significantly the performance at 4.5 K of MQXFS7d, an iteration with nominal azimuthal pre-load ($\sim$ 110 MPa). The "quench plateau" at 4.5 K in MQXFS7h and S7i is reduced after thermal cycle (by 140 A and 150 A respectively), and also after numerous current cycles to simulate mechanical fatigue (by 100 A and 50 A). After returning to lower pre-load, thermal and current cycling in MQXFS7j did not significantly change the performance of the magnet at 4.5 K.

B. Quench Origin

In Figs. 5 and 6, each quench is labeled with its start location. During the training of MQXFS7a at 1.9 K and 20 A/s, quenches occurred in all four coils, mainly in the inner layer pole block (I3-I4), the inner layer pole turn (I5-I6, I7-I8), and the layer jump (I8-O1) segments. During the re-training of MQXFS7h we also observed quenches in all four coils, in segment I3-I4 and also in the outer layer midplane block (O6-O7). During all other tests at 1.9 K, which did not feature significant training, the magnet quenched mainly in segment C207 O6-O7 for earlier iterations, and in segment C211 I7-I8 in MQXFS7j.

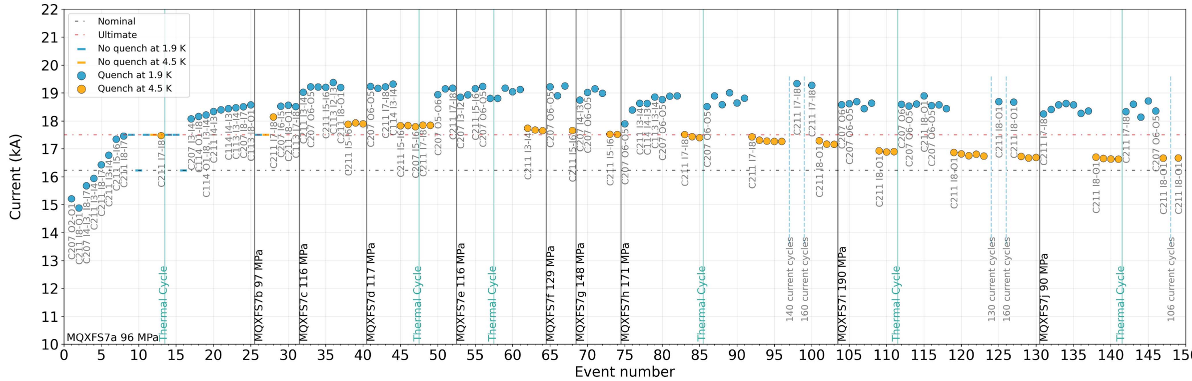

Fig. 5. Training history of MQXFS7, at the nominal ramp rate (20 A/s). Each magnet iteration is marked with a black vertical line. The quench location is indicated with a label next to the quench point, each time the quench location changed.

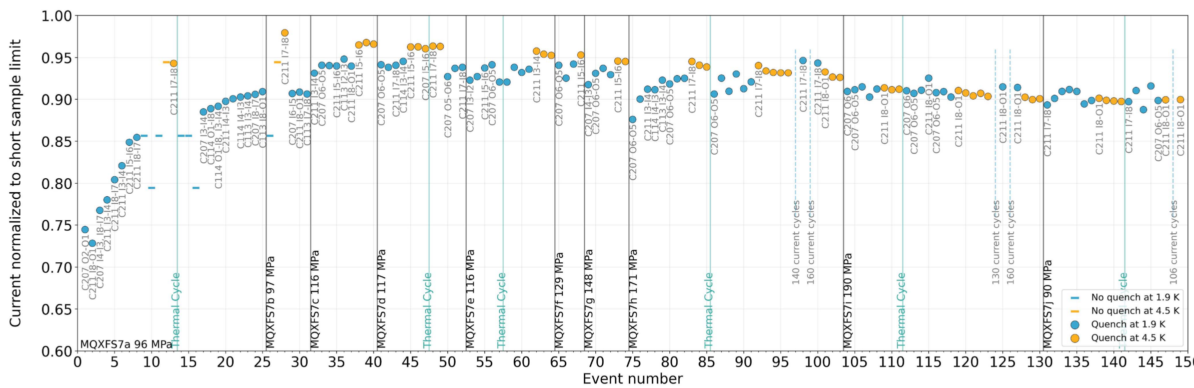

Fig. 6. Training history of MQXFS7, at the nominal ramp rate (20 A/s), current normalized to the short sample limit. Each magnet iteration is marked with a black vertical line. The quench location is indicated with a label next to the quench point, each time the quench location changed.

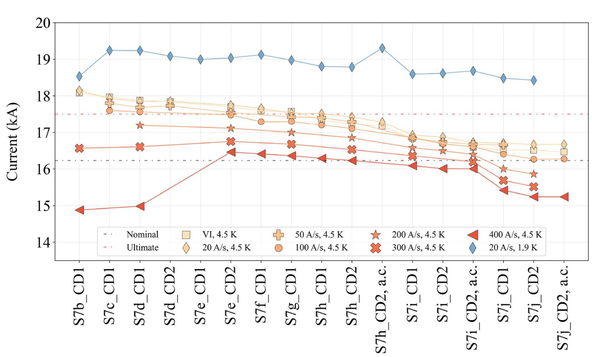

Fig. 7. Average quench level for each MQXFS7 iteration for different test temperatures and ramp rates. The CD number is the cool down number; tests after the current cycles are marked with "a.c.". The training "quench plateau" is shown as the data at 20 A/s, 1.9 K.

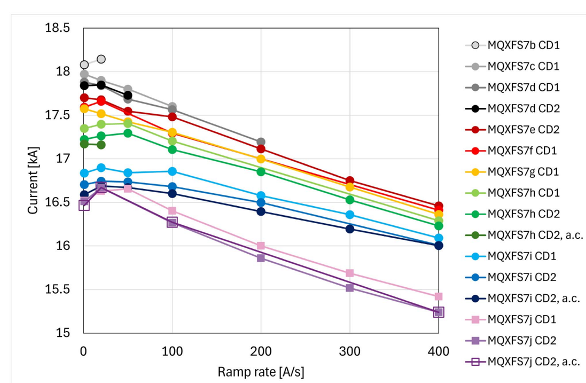

Fig. 8. Ramp rate dependency at 4.5 K in MQXFS7. The CD number is the cool down number; "a.c." corresponds to tests after the current cycles.

On the other hand, quenches at 4.5 K and 20 A/s are in coil 211in all but two cases. With the exception of MQXFS7e, which quenched in C211 I3-I4, the quenches start in the inner layer pole turn (C211 I5-I6 and C211 I7-I8) and layer jump (C211 I8-O1). These three segments are in the highest magnetic field region and therefore the margin to the critical current is smaller.

C. Ramp Rate Studies

The dependency of quench current on ramp rate at 4.5 K is shown in Fig. 8. The reduction of quench current after each iteration is observed at all ramp rates. After the highest pre-load level (MQXFS7i at 190 MPa), a larger change in quench current is observed at lower ramp rates. When going back to lower pre-load (MQXFS7j at 90 MPa), the change at lower ramp rates is

TABLE I
QUENCH LOCATION START IN THE RAMP RATE STUDIES AT 4.5 K IN MQXFS7

	Ramp rate [A/s]						
MQXFS7...	1	20	50	100	200	300	400
b, CD1	I3-I4	I7-I8	—	—	—	(207)	(114)
c, CD1	I5-I6	I5-I6	I5-I6	I5-I6	—	—	—
d, CD1	I7-I8	I5-I6	I5-I6	I5-I6	I5-I6	(207)	(114)
d, CD2	I7-I8	I7-I8	I5-I6	—	—	—	—
e, CD2	I3-I4	I3-I4	I3-I4	I3-I4	I3-I4	I3-I4	I3-I4
f, CD1	I5-I6	I5-I6	—	I5-I6	—	—	I5-I6
g, CD1	I7-I8	I5-I6	I5-I6	I5-I6	I5-I6	I5-I6	I5-I6
h, CD1	I7-I8	I7-I8	I5-I6	I5-I6	—	—	I5-I6
h, CD2	I7-I8	I7-I8	I7-I8	I7-I8	I5-I6	I5-I6	I5-I6
h, CD2, a.c.	I8-O1	I8-O1	—	—	—	—	—
i, CD1	I8-O1	I8-O1	I7-I8	I7-I8	I7-I8	I5-I6	I5-I6
i, CD2	I8-O1	I8-O1	I8-O1	I8-O1	I8-O1	—	I5-I6
i, CD2, a.c.	I8-O1	I8-O1	I8-O1	I8-O1	I8-O1	I8-O1	I7-I8
j, CD1	I8-O1	I8-O1	I8-O1	I7-I8	I7-I8	I7-I8	I7-I8
j, CD2	I8-O1	I8-O1	—	I7-I8	I7-I8	I7-I8	I7-I8
j, CD2, a.c.	I8-O1	I8-O1	—	I7-I8	—	—	I7-I8

Note: — indicates not done. The CD number is the cool down number.
"a.c." indicates after the current cycles test.
All quenches were in coil 211, unless noted.

not as large as previous iterations, but the change at higher ramp rates is the largest observed.

The quenches summarized in Fig. 8 started mainly in the same three locations as mentioned in Section III-B: C211 I5-I6, C211 I7-I8, and C211 I8-O1. In Table I the quench location at each ramp rate is shown for each MQXFS7 iteration. Note that, starting with MQXFS7f (the first iteration with higher than nominal pre-load), the quench location "moves" from C211 I5-I6 to C211 I7-I8 and then to C211 I8-O1 with succesive iterations, and that at higher ramp rates this "movement" is delayed with respect at lower ramp rates. When reaching back to lower pre-load in MQXFS7j, quenches in C211 I8-O1 are those for which the quench current changed least from MQXFS7i; while quenches at 100-400 A/s, that show the largest current change, went from I8-O1 to I7-I8.

D. V-I Measurements

To perform V-I measurements, a special stepwise current cycle was done in the magnet, with 5 min current steps every few kA at lower magnet current, with the step size reducing to 100 A near the quench current. The voltage between several pairs of voltage taps in the magnet were measured during the full current cycle. At each current step, for each signal, we extract the average voltage, and we calculate the error of the mean voltage at the 95% confidence level. The resulting average voltage versus current step level plot is the so-called *V-I plot* for a given coil segment. An example V-I plot for segment 211 I8-O1 is shown in Fig. 9, with measurements for several iterations of MQXFS7. All measurements reported in this section were done at 4.5 K.

The measured segments in coils 113, 114 and 207 did not show any voltage rise up to the maximum current reached in any of the MQXFS7 iterations tested, within $\sim$1 µV; in coil 211, voltages in the order of several µV were measured in several segments in steady-state before quenching.

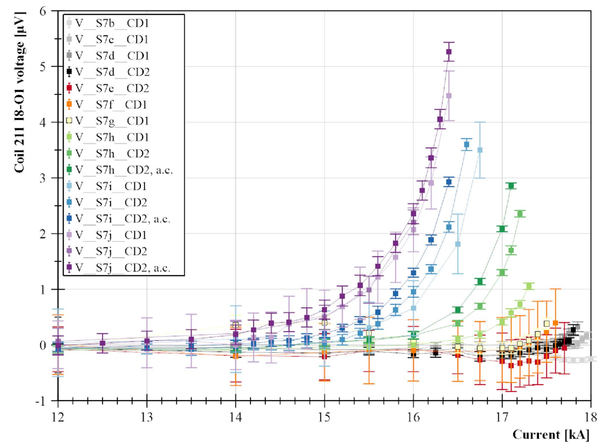

Fig. 9. All V-I measurements in segment C211 I8-O1 across MQXFS7 iterations, at 4.5 K. For reference, this segment is 0.29 m long. The fit from (1) was applied to each dataset to obtain the critical current shown in Fig. 10.

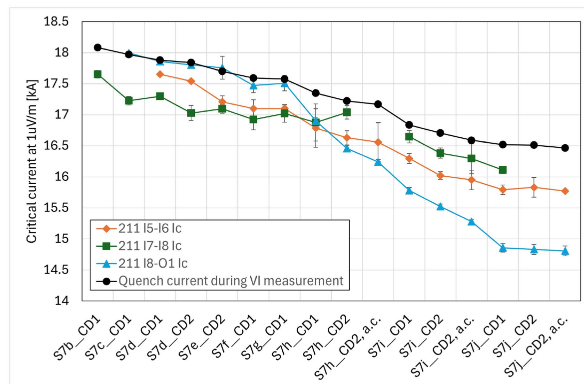

Fig. 10. Evolution of the critical current (calculated from 2), in three segments in coil 211, as function of MQXFS7 iteration and thermal cycling. The CD number is the cool down number; "a.c." corresponds to tests after the current cycles.

The direct measurements of the full coils were not exploitable due to the low signal to noise ratio; numerically bucking the measurements of the coils by subtracting the measurements of other coils reduced the error per current plateau to $\sim$2–3 µV. The comparison of coils 113, 114 and 207 with each other showed that the coil voltage differences remained roughly constant; the comparison of coil 211 with any of the other coils showed a clear voltage increase with current up to $\sim$10 µV.

In coil 211, the three segments that showed the largest voltage in their V-I plots were C211 I5-I6, I7-I8 and I8-O1. The length of these segments is 1.03, 0.72 and 0.29 m respectively. To evaluate the change in the V-I plots for these three segments, a non-linear fit of the data was done following this equation:

$$\frac{V}{1\mu\mathrm{V/m}\cdot l} = a_1 + a_2 \cdot \left(\frac{I}{I_{\max}}\right)^{a_3} \quad (1)$$

where V is the voltage, l is the length of the measured segment, I the current, $I_{\max}$ the maximum measured current, and a_1, a_2 and a_3 the fit parameters. Parameter a_1 represents a constant

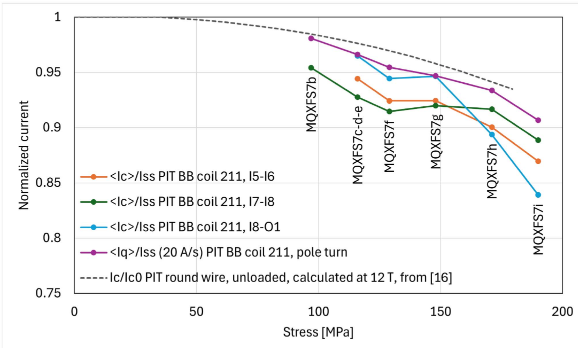

Fig. 11. Average critical current $\langle I_c \rangle$ in three segments in coil 211 and average quench current at 20 A/s $\langle I_q \rangle$ in these segments normalized to short sample limit (I_{ss}). The average is calculated at each pre-load level. For reference, the data for PIT round conductor at 4.2 K, extrapolated to 12 T [18] is shown as a dashed line.

TABLE II
PERFORMANCE OF EACH COIL IN MQXFS7 AT SEVERAL CONDITIONS

Coil	113	114	207	211
Conductor	RRP®	RRP®	PIT	PIT (BB)
I_{ss} (1.9 K)	22.2 kA	21.9 kA	21.1 kA	20.4 kA
I_{ss} (4.5 K)	20.1 kA	19.8 kA	19.2 kA	18.5 kA
At nominal pre-load (MQXFS7e)				
Quenched at 1.9 K	No	No	Yes	Yes
Quenched at 4.5 K	No	No	No	Yes
Maximum fraction of I_{ss}	88 %	90 %	92 %	96 %
Maximum V-I voltage	$\sim$0	$\sim$0	$\sim$0	$\sim$10 μV
At maximum pre-load (MQXFS7i)				
Quenched at 1.9 K	No	No	Yes	Yes
Quenched at 4.5 K	No	No	No	Yes
Maximum fraction of I_{ss}	84 %	85 %	88 %	91 %
Maximum V-I voltage	$\sim$0	$\sim$0	$\sim$0	$\sim$10 μV

Note: RRP® = Restacked Rod Process (Bruker OST); PIT = Powder-in-Tube (Bruker EAS); PIT (BB) = Powder-in-Tube with bundle barrier (Bruker EAS)

measurement offset. The normalization $I/I_{\max}$ is done to improve the numerical calculation. The critical current at 1 µV/m (I_c) can be calculated from a_2 and a_3 as:

$$I_c = \frac{I_{\max}}{a_2^{1/a_3}} \quad (2)$$

The evolution of this critical current over the different MQXFS7 iterations is shown in Fig. 10 .

IV. Discussion

Of the four coils in MQXFS7, we have only observed systematic performance degradation in one (coil 211). This finding is consistent with the most recent results obtained in single wire tests under transverse compressive loads [18], [19], where the strain sensitivity of PIT conductors has been found to be larger than that of their RRP counterparts. In Table II we summarize the maximum measured performance of each coil at several conditions.

In coil 211, three coil segments show the most significant performance change: I5-I6, I7-I8 and I8-O1. The first two segments are the inner layer pole turn straight section, and the last one is the layer jump. In Fig. 11 the average (at each pre-load level) critical current and quench current at 20 A/s, normalized to the short sample limit, is shown as function of the pre-load. As reference, the critical current normalized to the initial critical current of a 1 mm PIT wire without bundle barrier at 4.2 K from [18], extrapolated to 12 T is shown in the same plot. The performance indicators from the PIT BB coil 211 follow closely the measurements on the PIT wire.

V. Conclusion

A MQXF short model, composed of two RRP Nb_3Sn coils, one PIT Nb_3Sn coil without bundle barrier, and one PIT Nb_3Sn coil with bundle barrier, was extensively tested at the CERN magnet test facility SM18. The magnet, whose nominal azimuthal pre-load is 110 MPa, was pushed to a maximum of 190 MPa, and experienced a total of 15 cool downs to liquid helium temperatures.

Throughout this test campaign, the two RRP coils did not show any reduction of performance up to the maximum current they reached. At the maximum pre-load of 190 MPa, these coils did not quench nor show an initial superconductor to normal transition up to 84-85% of their short sample limit. The PIT coil without bundle barrier, while it quenched at 1.9 K, also showed no start of the superconductor to normal transition up to 88% of its short sample limit at 190 MPa. Since the magnet was limited by the fourth coil, any potential degradation in the other three coils above $\sim$ 90% of their short sample limit could not be detected.

The quench limitation was on the fourth coil, a coil wound with PIT bundle barrier cable, with a lower short sample limit. This coil reached 98% of short sample limit in initial iterations of MQXFS7, and at the maximum pre-load iteration it reached a maximum of 91% of short sample limit. At this maximum pre-load level, the superconductor to normal transition in this coil was well visible at 84, 87 and 88% of its short sample limit in three short segments in and near the inner pole turn (the highest field region), respectively.

At the very high pre-load levels (170 and 190 MPa), the performance of the magnet reduced after thermal cycles and current cycles simulating mechanical fatigue, while thermal and current cycling at or below nominal pre-load level (110 MPa) did not change the performance of the magnet.

An in-depth investigation of the performance change in this coil was done, comparing when possible with measurements done in PIT strands under high stresses. This investigation showed that the reduction of the PIT BB coil performance (in terms of quench current and critical current) was of the same order of magnitudes as the measurements in PIT strands.

Acknowledgment

The authors thank the HL-LHC project and HFM program for supporting this study. The authors also thank S. Hopkins for his insightful feedback and C. Senatore for valuable discussions and sharing his data used in Fig. 11.

REFERENCES

[1] E. Todesco et al., "A first baseline for the magnets in the high luminosity LHC insertion regions," *IEEE Trans. Appl. Supercond.*, vol. 24, no. 3, Jun. 2014, Art. no. 4003305.

[2] S. Caspi et al., "The use of pressurized bladders for stress control of superconducting magnets," *IEEE Trans. Appl. Supercond.*, vol. 11, no. 1, pp. 2272–2275, Mar. 2001.

[3] G. Vallone and P. Ferracin, "Modeling coil-pole debonding in $\mathrm{Nb_3Sn}$ superconducting magnets for particle accelerators," *IEEE Trans. Appl. Supercond.*, vol. 27, no. 8, Dec. 2017, Art. no. 4004611.

[4] G. Chlachidze et al., "Performance of the first short model 150-mm-Aperture Nb3Sn quadrupole MQXFS for the high-luminosity LHC upgrade," *IEEE Trans. Appl. Supercond.*, vol. 27, no. 4, Jun. 2017, Art. no. 4000205.

[5] S. Stoynev et al., "Summary of test results of MQXFS1—The first short model 150mm aperture Nb3Sn quadrupole for the high-luminosity LHC upgrade," *IEEE Trans. Appl. Supercond.*, vol. 28, no. 3, Apr. 2018, Art. no. 4001705.

[6] H. Bajas et al., "Test result of the short models MQXFS3 and MQXFS5 for the HL-LHC upgrade," *IEEE Trans. Appl. Supercond.*, vol. 28, no. 3, Apr. 2018, Art. no. 4007006.

[7] F. Mangiarotti et al., "Test results of the CERN HL-LHC low-β quadrupole short models MQXFS3c and MQXFS4," *IEEE Trans. Appl. Supercond.*, vol. 29, no. 5, Aug. 2019, Art. no. 4001705.

[8] F. J. Mangiarotti et al., "Powering performance and endurance beyond design limits of HL-LHC low-beta quadrupole model magnets," *IEEE Trans. Appl. Supercond.*, vol. 31, no. 5, Aug. 2021, Art. no. 4000805.

[9] J. F. Troitino et al., "Optimizing the use of pressurized bladders for the assembly of HL-LHC MQXFB magnets," *Superconductor Sci. Technol.*, vol. 36, no. 7, 2023, Art. no. 065002.

[10] S. I. Bermudez et al., "Performance of a MQXF Nb3Sn quadrupole magnet under different stress level," *IEEE Trans. Appl. Supercond.*, vol. 32, no. 6, Sep. 2022, Art. no. 4007106.

[11] L. D. Cooley, A. K. Ghosh, D. R. Dietderich, and I. Pong, "Conductor specification and validation for high-luminosity LHC quadrupole magnets," *IEEE Trans. Appl. Supercond.*, vol. 27, no. 4, Jun. 2017, Art. no. 6000505.

[12] B. Bordini et al., "The bundle-barrier PIT wire developed for the HiLumi LHC project," *IEEE Trans. Appl. Supercond.*, vol. 27, no. 4, Jun. 2017, Art. no. 6000706.

[13] H. Prin et al., "First CERN cold masses for the HL-LHC interaction regions," *IEEE Trans. Appl. Supercond.*, vol. 34, no. 5, Aug. 2024, Art. no. 4004805.

[14] G. Vallone et al., "Summary of the mechanical performances of the 1.5m long models of the $\mathrm{Nb_3Sn}$ low-β quadrupole MQXF," *IEEE Trans. Appl. Supercond.*, vol. 29, no. 5, Aug. 2019, Art. no. 4002805.

[15] E. Takala et al., "Mechanical comparison of short models of Nb3 sn Low-β quadrupole for the Hi-Lumi LHC," *IEEE Trans. Appl. Supercond.*, vol. 31, no. 5, Aug. 2021, Art. no. 4000306.

[16] A. Chiuchiolo et al., "Strain measurements with fiber bragg grating sensors in the short models of the HiLumi LHC low-beta quadrupole magnet MQXF," *IEEE Trans. Appl. Supercond.*, vol. 28, no. 4, Jun. 2018, Art. no. 4007805.

[17] E. Ravaioli, "CLIQ. A new quench protection technology for superconducting magnets," Ph.D. dissertation, University of Twente, 2015, doi: 10.3990/1.9789036539081.

[18] C. Senatore, T. Bagni, J. Ferradas-Troitino, B. Bordini, and A. Ballarino, "Degradation of I_c due to residual stress in high-performance $\mathrm{Nb_3Sn}$ wires submitted to compressive transverse force," *Supercond. Sci. Technol.*, vol. 36, no. 7, 2023, Art. no. 075001.

[19] D. Baffari and B. Bordini, "Effect of the sub-elements layout on the electro-mechanical properties of high Jc Nb3Sn wires under transverse load: Numerical simulations," *IEEE Trans. Appl. Supercond.*, vol. 32, no. 6, Sep. 2022, Art. no. 6001306.